# Fluorescence of the retinal chromophore in microbial and animal rhodopsins

Dmitrii M. Nikolaev[1], Andrey A. Shtyrov[1], Sergey Yu. Vyazmin[2], Andrey V. Vasin[3], Maxim S. Panov[1,4], Mikhail N. Ryazantsev[1,*]

1 Institute of Chemistry, Saint Petersburg State University, 26 Universitetskii pr, St. Petersburg, 198504, Russian Federation
2 Saint Petersburg Academic University, 8/3 Khlopina Street, St. Petersburg, 194021, Russian Federation
3 Institute of Biomedical Systems and Biotechnologies, Peter the Great St. Petersburg Polytechnic University, 29 Polytechnicheskaya Str., St. Petersburg, 195251, Russian Federation
4 St. Petersburg State Chemical Pharmaceutical University, Professor Popov str., 14, lit. A, St. Petersburg, 197022, Russian Federation

* mikhail.n.ryazantsev@gmail.com

## Abstract

Fluorescence of the vast majority of natural opsin-based photoactive proteins is extremely low in accordance with their functions that depend on efficient transduction of absorbed light energy. However, recently proposed several classes of engineered rhodopsins with enhanced fluorescence along with the discovery of a new natural highly fluorescent rhodopsin, NeoR, opened a way to exploit these transmembrane proteins as fluorescent sensors and draw more attention to studies on this untypical rhodopsins property. Here we review available data on the fluorescence of the retinal chromophore in microbial and animal rhodopsins and their photocycle intermediates as well as different isomers of the protonated retinal Schiff base in different solvents and the gas phase.

## Introduction

Rhodopsins are heptahelical photosensitive membrane-embedded proteins that have been found in organisms from all domains of life [1–6]. Rhodopsin functioning cycle starts with light absorption by the retinal cofactor, which is covalently bound to the conserved lysine of apoprotein via the Schiff base linkage. Photon absorption converts the retinal to the first excited state, and the decay to the ground state can proceed either through non-radiative or radiative pathways. The non-radiative decay goes through a conical intersection where the branching of photoreaction occurs. The first path converts the chromophore back to the initial form, the second path leads to the successful photoisomerization reaction that initiates a series of processes required for rhodopsin to perform its function. Protein environment of rhodopsins facilitates the photoisomerization since it is directly related to rhodopsin functioning, and this process occurs very efficiently (e.g. photoisomerization quantum yields in bovine visual rhodopsin and bacteriorhodopsin are 0.65 and 0.64, respectively) [7–9]. On the contrary, fluorescence is a side process for rhodopsins functioning, and the radiative pathway is suppressed in these proteins. Observed fluorescence quantum yields of microbial and



https://doi.org/10.26434/chemrxiv-2023-3n1d0 ORCID: https://orcid.org/0000-0003-3413-1706 Content not peer-reviewed by ChemRxiv. License: CC BY-NC-ND 4.0

animal rhodopsins are extremely low, with a single exception of the recently discovered neorhodopsin (NeoR) from *Rhizoclosmatium globosum* [10–12].

Recent studies on the application of microbial rhodopsins as fluorescence voltage indicators in optogenetics facilitated the development of bright rhodopsin variants. Directed evolution approach has allowed the researchers to obtain rhodopsin mutants with significantly more intense fluorescence than observed in the wild-type rhodopsins at physiological pH, and engineered proteins have been successfully applied in a large number of biological and medical studies [13–20]. Increasing number of applications of bright rhodopsin variants have raised the interest in rhodopsins fluorescence properties [21–23]. In this review we compile, systematize, and analyze experimental data obtained for fluorescence properties of rhodopsins that are available in literature. The studies on microbial and animal rhodopsins and their mutants, rhodopsin photocycle intermediates, and also retinal protonated Schiff base in solvents and the gas phase are considered.

## Fluorescence properties of microbial rhodopsins

Microbial rhodopsins that include type 1 rhodopsins and recently discovered heliorhodopsins, perform versatile functions in unicellular microorganisms and viruses, acting as light-driven ion pumps, ion channels, enzymes, or sensors. Microbial rhodopsins are also a key tool in optogenetics used for activation, silencing, or monitoring electrical activity of cells under light control, and non-natural variants are actively developed for these purposes. As the photosensitive cofactor, chromophore, most microbial rhodopsins utilize 13-*trans*, 15-*anti* retinal. For fluorescence properties of microbial rhodopsins, in contrast to the animal opsin-based photoreceptive proteins discussed in the next section, a substantial amount of data are available. These data are compiled in Table 1 and represented graphically in Figures 1a, b and 3a, b. Table 1 contains fluorescence excitation maxima ($\lambda_{exc}$), maxima of fluorescence band ($\lambda_{em}$), quantum yields of fluorescence ($\Phi$), and excited state lifetimes ($\tau_f$) that are reported for wild-type microbial rhodopsins and their mutants measured in a wide range of pH as well as for the O and Q intermediates of bacteriorhodopsin.

*Fluorescence quantum yields and fluorescence lifetimes.* Figure 1a shows plots of the fluorescence quantum yields logarithm ($\log \Phi$) as a function of corresponding absorption band maxima ($\lambda_{abs}$). The plot is color-coded in the following way. The data for wild-type microbial rhodopsins measured at physiological pH are represented by blue points. The green color is used to represent data for wild-type microbial rhodopsins measured at pH other than physiological as well as for mutants except the data for highly fluorescent engineered rhodopsins that are shown in brown. Finally, the light blue point in the figures represents the O photocycle intermediate of bacteriorhodopsin. The fluorescence quantum yield of a recently discovered NeoR ($\Phi = 0.2$) stands out significantly among the rest of microbial rhodopsins and the corresponding point is omitted in Figure 1a and the values are given only in Table 1.

Fluorescence quantum yields of discussed rhodopsins vary in a wide range. A tendency of increasing fluorescence quantum yield together with increasing of absorption band maximum (but not a strong correlation) can be clearly seen from the plot. This observation suggests that the same factors might be involved in the tuning of these properties. $\Phi$ values for the majority of wild-type microbial rhodopsins at physiological pH have the same order of magnitude $\sim 10^{-4}$. The fluorescence quantum yield substantially increases for the acidic forms of bacteriorhodopsin (bR blue, $\Phi = 4.5 \cdot 10^{-3}$) and sensory rhodopsin I (SRI pH6, $\Phi = 1.3 \cdot 10^{-3}$) reaching the next order of magnitude. The same increase was found for the O and Q photocycle intermediates of bacteriorhodopsin with quantum yields of $\approx 1 \cdot 10^{-3}$ and $7 \cdot 10^{-3}$, respectively. Because $\lambda_{abs}$ is not measured for the Q intermediate the corresponding point is not shown in Figure 1. Fluorescence



https://doi.org/10.26434/chemrxiv-2023-3n1d0 **ORCID:** https://orcid.org/0000-0003-3413-1706 Content not peer-reviewed by ChemRxiv. **License:** CC BY-NC-ND 4.0

quantum yields for three engineered bright variants (Archer1, QuasAr1, and GR D121A) fall in the $\sim 10^{-3}$ region and even achieve the next order of magnitude for Archon2 ($\Phi = 1.05 \cdot 10^{-2}$).

A similar picture can be observed for fluorescence lifetimes of microbial rhodopsins (Table 1). The data are visualized in Figure 1b, where logarithms of fluorescence lifetimes $\log(\tau_f)$ are plotted as a function of corresponding absorption band maxima ($\lambda_{abs}$). Again, the points representing the engineered archaerhodopsin-3 mutants (QuasAr1 and Archon2), the O intermediate of bR, two microbial rhodopsins at lower pH (SRI pH6, bR R82Q pH4), and two bR mutants with a substituted counterion (bR D85S, bR D85N) are located above the wild-type rhodopsins at neutral pH and shifted to the right side of the figure. Engineered bright archaerhodopsin-3 mutants QuasAr1 and Archon2 are located in the top of the figure, i.e. they demonstrate the largest values of $\tau_f$ reported to date.

Clearly, the observed variety of fluorescence properties of opsin-based photoreceptors that bear the same chromophore is determined by difference in the interaction of this chromophore with its environment. The role of such interaction in tuning rhodopsins absorption band maxima is investigated in many studies (e.g. [24–28]). The electrostatic and steric parts of the protein-chromophore interaction are found to be the most important, although in some computational studies [24] non-negligible transfer of electron density between the chromophore and surrounding amino acids was also detected. The most significant color determinant is the electrostatic effect of counterions, the negatively charged amino acids situated in the vicinity of the positively charged $^{+}$N-H part of the chromophore, e.g. two titratable residues, D85 and D212, in bacteriorhodopsin (Figure 2a). It was shown both experimentally and based on computational models that a substitution of a counterion by a neutral residue or the protonation of this counterion leads to a significant red shift of the absorption band maximum. The key role of the counterion electrostatic effect for rhodopsins fluorescent properties is also evident from available experimental data. Indeed, the data compiled in Figures 1a, b clearly demonstrates the increase in the fluorescence quantum yields and fluorescence lifetimes with the transition from the ground form of wild-type microbial rhodopsins to the mutants with a counterion substituted by a neutral amino acid or to the form with neutralized protonated counterion.

Available data on the pH dependence of fluorescent properties also confirm the connection of the counterion protonation state with fluorescence and photoisomerization efficiency. In the study on bacteriorhodopsin [29], a significant increase of fluorescence intensity was detected at acidic pH values with the most intense emission at pH around 1.7 ($\approx$ 15-fold enhancement compared to neutral pH). Observed pH-dependence of fluorescence intensity correlates with the pH-dependence of the absorption band maximum that shifts to the longer wavelength region upon acidification. On the contrary, only negligible changes in fluorescence intensity and absorption band maximum were observed in the alkaline pH range. These findings are in line with the pKa value $\approx 2.7$ reported for the bacteriorhodopsin counterion D85 [30]. In a recent time resolved spectroscopy study on bacteriorhodopsin [31], a slow decay component ($\tau_f = 7.8$ ps) arising at low pH<4 has been detected and assigned to the state with protonated counterion (the blue form, Figure 2b). Similarly, emission intensity enhancement upon lowering pH value was found for *Gloebacter violaceus* rhodopsin [32], xanthorhodopsin [33], *Exiguobacterium sibiricum* rhodopsin (ESR) [34], and elongation of excited state lifetime upon acidification was reported for proteorhodopsin (PR) [31, 35, 36] and Krokinobacter rhodopsin 2 [37].

In all cases, increase of fluorescence quantum yields or excited state lifetimes occurs in the region close to the pKa of the counterion. Moreover, it was demonstrated that fluorescence intensity can be changed by tuning the counterion pKa [34, 38]. For instance,



https://doi.org/10.26434/chemrxiv-2023-3n1d0 **ORCID:** https://orcid.org/0000-0003-3413-1706 Content not peer-reviewed by ChemRxiv. **License:** CC BY-NC-ND 4.0

in the study [38] the pKa of the D85 counterion in bacteriorhodopsin was raised up to $\approx 7.5$ by a substitution of the positively charged arginine R82 with a polar glutamine residue. Accordingly, a significant elongation of excited state decay was observed upon lowering pH value from 9.6 (0.6 ps) to 4.4 (biphasic decay, equally contributing components with lifetimes 2.0 and 7.0 ps). In the study [34] different magnitudes of fluorescence intensity increase were observed upon lowering pH value for wild-type ESR and its H57M mutant. In the wild-type protein with the pKa of D85 counterion estimated to be $< 2$ lowering pH from 7 to 5 resulted in a 2-fold emission enhancement. When a histidine, which strongly interacts with the D85 counterion in ESR, was substituted with methionine, a large increase of pKa(D85) up to 6.3 and, accordingly, an approximately 100-fold increase of fluorescence intensity upon lowering pH from 9 to 4.5 was observed.

Increase of the counterion pKa and, subsequently, enhancement of the fluorescence was also observed for the O intermediate of the bacteriorhodopsin photocycle. The O intermediate arises at the last stage of the photocycle and converts to the ground state of the protein on the timescale of $\approx 10$ ms [39, 40]. The main difference between the O intermediate and the ground state is the protonation state of two titratable groups – the D85 counterion and the proton release group [40] located close to the extracellular side of the protein that includes E194, E204, R82, Y83, and surrounding water molecules as shown in Figure 2c. In the O intermediate, the proton is located on the counterion, and it is transferred to the proton release group during the O $\rightarrow$ ground state transition. As suggested in a recent computational investigation [41], the proton transfer can proceed through the chain of water molecules shown in Figure 2c. While the direct experimental measurements of the counterion pKa in the O intermediate were not reported, a titration of bacteriorhodopsin showed that when proton release group is deprotonated, the pKa of the counterion raises up to $\approx 7.5$ [42]. Accordingly, fluorescence quantum yield ($\approx 1 \cdot 10^{-3}$) and lifetime ($9 \pm 2$ ps) of O intermediate at neutral pH are closer to the bacteriorhodopsin (pKa(D85) $\approx 2.7$) at pH $\approx 2$ (blue form) than at neutral pH.

Another fluorescent transient species, the Q intermediate, was detected by time-resolved fluorescence spectroscopy as the species with long-lived fluorescence ($62 \pm 2$ ps) [43–45]; its fluorescence quantum yield was measured to be $7 \cdot 10^{-3}$, which is 7 times larger than the value for the O intermediate. The Q intermediate is not involved in the main photocycle of bacteriorhodopsin, but rather produced upon photoexcitation of the N intermediate [44]. The structure and protonation state of titratable residues of Q intermediate have not been determined, but the observed long-lived fluorescence allows us to suggest that the counterion in this form is protonated.

Long-lived fluorescence of photocycle intermediates is also detected for archaerhodopsin-3 [23,46], *N. pharaonius* halorhodopsin, Krokinobacter rhodopsin 2 (KR2), and rhodopsin from *Rubrobacter xylanophilus* (RxR) [23]. Under low intensity of a light source, only a dim fluorescence, which can be attributed to the ground state, is observed. However, under intense illumination favoring accumulation of photocycle intermediates, the fluorescence signal substantially increases. This intense fluorescence can be characterized by a bi-exponential decay with smaller and bigger components, $\tau_1$ and $\tau_2$ (Table 1). For the investigated rhodopsins, the $\tau_1$ and $\tau_2$ components range from 5.2 to 9.6 ps and from 24 to 60 ps, respectively. These values are similar to the lifetimes reported for the O and Q bacteriorhodopsin intermediates and also can be attributed to the lifetimes for the O and Q states of the studied proteins.

For bright archaerhodopsin-3 mutants (Archer1, QuasAr1, and Archon2), which are nowadays widely used as genetically-encoded voltage indicators, the origin of fluorescence enhancement is not completely understood yet. In QuasAr1 and Archon2, one of the counterions, D95, is substituted with glutamine and histidine, respectively, but the protonation state of the second counterion, D222, has not been investigated. Intense fluorescence of these proteins at physiological pH may also indicate the elevated pKa



https://doi.org/10.26434/chemrxiv-2023-3n1d0 **ORCID:** https://orcid.org/0000-0003-3413-1706 Content not peer-reviewed by ChemRxiv. **License:** CC BY-NC-ND 4.0

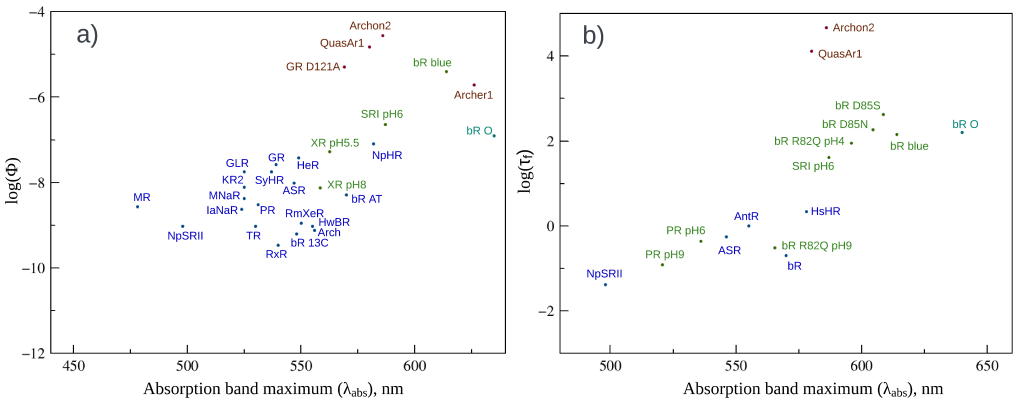


**Figure 1.** a) Fluorescence quantum yields logarithm (log Φ) of microbial rhodopsins as a function of absorption band maxima ($\lambda_{abs}$). b) Fluorescence lifetimes logarithm (log $\tau_f$) of microbial rhodopsins as a function of $\lambda_{abs}$. Wild type microbial rhodopsins at physiological pH are shown in blue. Microbial rhodopsin at non-physiological pH and rhodopsin mutants except engineered bright mutants are shown in green. Bacteriorhodopsin O photocycle intermediate is shown in light blue. Bright mutants of archaerhodopsin-3 and *Gloebacter violaceus* rhodopsin are shown in brown. For abbreviations of proteins, see Table 1.

value of the remaining counterion and, consequently, its protonation. For Archer1, the increase of the counterion pKa up to 8.9 also has been recently demonstrated [47].

*Fluorescence emission and excitation bands maxima and Stokes shifts.* For majority of the discussed rhodopsins, the excitation band maximum $\lambda_{ex}$, i.e. an excitation wavelength at which the arising fluorescence is the most intense, is very similar to the absorption band maximum $\lambda_{abs}$ of the corresponding rhodopsin (Table 1). This observation is of particular importance for engineered bright rhodopsins QuasAr1 and Archer1 confirming that the fluorescence originates from the ground state but not from intermediates.

Two microbial rhodopsins, however, stand out from the rest. For *E. sibiricum* rhodopsin, the fluorescence excitation band is found to be red-shifted relative to the absorption band ($\lambda_{abs}$ = 531 nm, $\lambda_{exc}$ = 556 nm at pH = 7) [34]. To explain this finding, in the study [34] the excitation band was deconvoluted into two components. The red-shifted component (564 nm) was assigned to the brighter species with the protonated counterion D85 and the blue-shifted component (531 nm) was assigned to the dim species with the counterion at its deprotonated state. In line with this assumption, $\lambda_{em}$ is shifting closer to $\lambda_{abs}$ at more alkaline pH ($\lambda_{exc}$ = 538 nm, $\lambda_{abs}$ = 531 nm, pH = 8.8). Besides, for ESR D85N mutant where the counterion is substituted with a polar residue $\lambda_{exc}$ (564 nm) and $\lambda_{abs}$ (563 nm) are almost identical to the $\lambda_{exc}$ of the red-shifted component of the wild-type protein.

The observed shift of excitation and absorption bands for proteorhodopsin at pH = 7 ($\lambda_{abs}$ = 531 nm, $\lambda_{exc}$ = 564 nm ) [35] can be also explained by coexisting states with the protonated and deprotonated counterion D97, which is in full agreement with its reported pKa value of $\sim$ 7.0 [50, 51] and the multi-phasic decays of the excited-state population of this rhodopsin discussed in recent studies [31, 36].

The emission band maxima of microbial rhodopsins demonstrate a general trend of increasing $\lambda_{em}$ upon red-shifting absorption band maxima (Figure 3a, but the linear correlation is moderate. The coefficient of determination $R^2$ is 0.73 if the data for NeoR were not included in the data set. However, for Stokes shifts (in kcal/mol) plotted as a function of $\lambda_{abs}$, the linear correlation is much better (Figure 3b). For this plot, the



https://doi.org/10.26434/chemrxiv-2023-3n1d0 **ORCID:** https://orcid.org/0000-0003-3413-1706 Content not peer-reviewed by ChemRxiv. **License:** CC BY-NC-ND 4.0

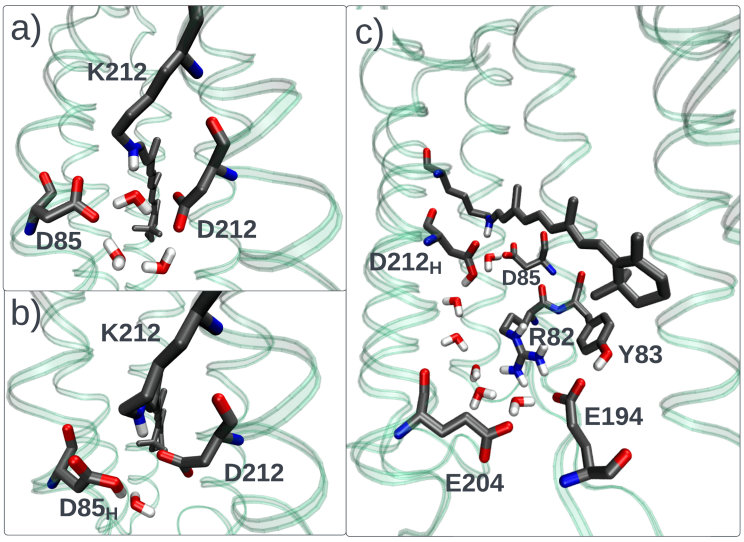


**Figure 2.** a) The pentagonal cluster composed of two counterions (D85 and D212) and three water molecules in the vicinity of the Schiff base of bacteriorhodopsin at a physiological pH. The structure was taken from Ref. [48]. b) The same region of bacteriorhodopsin at pH $\approx 2$ (the blue form of bacteriorhodopsin). c) The structure of bacteriorhodopsin O intermediate. The structure was constructed using homology modeling [49] based on the X-ray structure of O intermediate of bacteriorhodopsin L93A mutant (PDB ID 3VI0).

point corresponding to NeoR agrees perfectly with the rest of microbial rhodopsins, and the coefficient of determination $R^2$ derived for the complete set is 0.86.

## Animal opsin-based photoreceptors

Animal opsin-based photoreceptors perform a variety of roles related to sensation of light, such as vision, control of circadian rhythms, change of body color, etc. In majority of cases, light-activated functioning cycle of animal opsin-based photoreceptors involves the formation of the active state, which binds G-protein to launch signal transduction cascades [8, 39]. Similar to microbial rhodopsins, the central role in the photoactivation of animal opsin-based photoreceptors plays a chromophore that captures a photon and undergoes isomerization to start the corresponding photocycle. To date, four types of chromophores have been identified in animal opsin-based photoreceptors. In addition to retinal, 11-*cis* 3,4-dehydroretinal was found in visual opsin-based photoreceptors of fresh-water vertebrates, and 11-*cis* 3-hydroxy- and 4-hydroxyretinal were found in photoreceptors of invertebrates.

*Monostable animal opsin-based photoreceptors.* In monostable animal opsin-based photoreceptors, the active state is thermally unstable and its deactivation involves release of the chromophore. Subsequently, the original inactive state is regenerated when opsin binds a chromophore from the medium [6, 39, 52]. The main representatives of monostable opsin-based photoreceptors are the visual rhodopsins of vertebrates. Available experimental results on fluorescent properties of monostable rhodopsins are scarce and available, to our knowledge, only for the bovine visual rhodopsin containing 11-*cis* retinal chromophore and its analogue with 9-*cis* retinal, isorhodopsin.

The excited state decay of purified samples of bovine rhodopsin investigated with femtosecond up-conversion fluorescence spectroscopy was found to contain components



https://doi.org/10.26434/chemrxiv-2023-3n1d0 **ORCID:** https://orcid.org/0000-0003-3413-1706 Content not peer-reviewed by ChemRxiv. **License:** CC BY-NC-ND 4.0

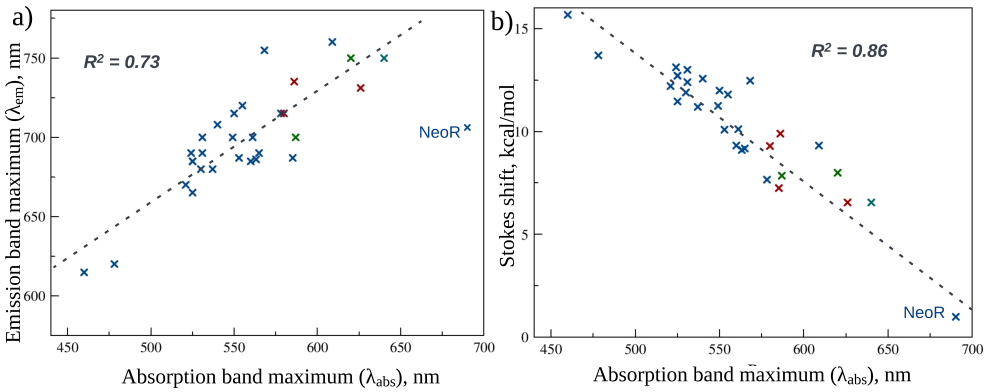


**Figure 3.** a) Emission band maxima ($\lambda_{em}$) of microbial rhodopsins as a function of absorption band maxima ($\lambda_{abs}$). The data were fitted by the least squares method (the black dotted line), the point corresponding to NeoR was excluded from the data set. The color code is defined as in Figure 1. b) Stokes shifts (in kcal/mol) of microbial rhodopsins as a function of $\lambda_{abs}$. The data were fitted by the least squares method (the black dotted line). The color code is defined as in Figure 1.

with lifetimes 0.146, 1.5, and 50 ps [53]. The 0.146 ps component with the largest contribution (80%) agrees with the fluorescence lifetime $\approx 0.1$ ps, which was evaluated using the fluorescence quantum yield value ($\Phi = 1.3 \pm 0.4 \cdot 10^{-5}$) measured for rod outer segments by a comparative method with erythrosin as a reference [54]. In the same up-conversion experiment, the repeated excitation of purified rhodopsin samples resulted in a linear dependence of the fluorescence intensity on the excitation power that indicates that photocycle intermediates do not contribute into fluorescent signal [53]. This observation is in line with results obtained in an earlier study [55], which detected fluorescence of bovine rhodopsin photocycle intermediates, but evaluated it to be much lower than fluorescence of the ground state form of rhodopsin photocycle. The fluorescence quantum yield of isorhodopsin was found to be only 2-fold larger compared to that of rhodopsin [56]. Thus, the fluorescence detected in the bovine rhodopsin and isorhodopsin is even less intense than the fluorescence of the wild-type microbial rhodopsins and the corresponding black points are located in the bottom left corner in Figure 4 a,b.

*Bistable animal opsin-based photoreceptors.* Just as monostable animal opsin-based photoreceptors, bistable animal opsins bind a retinal chromophore that captures light to initiate G protein-mediated phototransduction cascades. However, for this type of opsin-based photoactive proteins, a release of the retinal chromophore and bleaching do not occur during the photocycle but another thermally stable photoproduct, metarhodopsin, forms instead. Absorption of a second photon can convert metarhodopsin back to the ground state form. Irradiation with light of different wavelengths allows controlling the ratio of these two forms in the photostationary state. Bistable animal opsin-based photoactive proteins are widely spread in animal world and serve not only as visual receptors of invertebrates but also perform many other functions [39, 57, 58].

As is the case with vertebrate visual pigments, the available data on fluorescence properties of animal bistable opsins are much more scarce than for microbial rhodopsins (Table 2). So far, to our knowledge, the fluorescence quantum yields are measured only for the ground state of squid visual rhodopsin [54] and for the meta-form of visual rhodopsin in crayfish [59]; fluorescence lifetimes are reported for the ground states of squid [54] and octopus rhodopsins [60]. All mentioned opsins bind 11-*cis* retinal in their ground state that photoisomerizes to the all-*trans* isomer in corresponding metarhodopsins. The quantum yield measured for the ground state of squid rhodopsin that was extracted from



https://doi.org/10.26434/chemrxiv-2023-3n1d0 ORCID: https://orcid.org/0000-0003-3413-1706 Content not peer-reviewed by ChemRxiv. License: CC BY-NC-ND 4.0

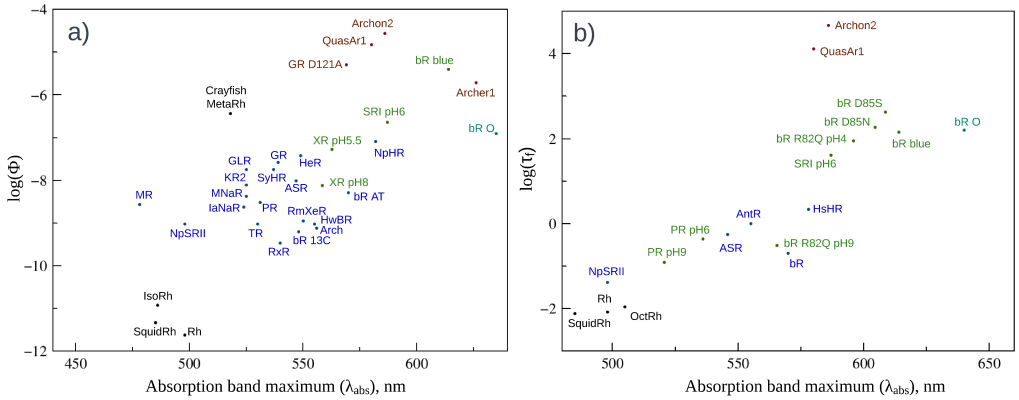


**Figure 4.** a) Fluorescence quantum yields logarithm (log Φ) of microbial and animal rhodopsins as a function of absorption band maxima ($\lambda_{abs}$). b) Fluorescence lifetimes logarithm (log $\tau_f$) of microbial and animal rhodopsins as a function of $\lambda_{abs}$. Animal rhodopsins and their photocycle intermediates are shown in black. The color code for microbial rhodopsins is defined as in Figure 1. For abbreviations of proteins, see Tables 1 and 2.

eyes of this invertebrate species was found to be $\Phi = 1.2 \cdot 10^{-5}$ [54] (a black point in the bottom left corner of Figure 4a and Table 2). This number is lower than fluorescence quantum yields of bacteriorhodopsin and comparable with quantum yields of bovine rhodopsin and isorhodopsin. On the contrary, the fluorescence quantum yield of the crayfish metarhodopsin recorded by microspectrofluorometry from isolated photoreceptor organelles (rhabdoms) at neutral pH 7.5 is considerably higher ($\Phi = 1.6 \pm 0.4 \cdot 10^{-3}$ [59]) and the corresponding black point in Figure 4a lies far above the points that represent ground states of both natural microbial and visual rhodopsins at physiological pH and closer to the points that correspond to the bacteriorhodopsin O intermediate, the acidic form of bacteriorhodopsin, and the engineered fluorescent mutants of microbial rhodopsins. Although fluorescence quantum yield for the ground state of the crayfish visual rhodopsin was not reported either in the discussed study [59] or in more recent studies, the authors also performed a thorough investigation to conclude that the fluorescence of the dark-adapted sample, i.e. the ground state of crayfish rhodopsin, was much lower than the fluorescence of the light-adapted sample and could not be detected with techniques applied in this study.

Similar substantial increase in fluorescence of meta states comparing to the ground state was observed also in *in vivo* microspectrofluorometric studies on the housefly [61] (*Musca domestica*), Drosophila [62] (*Drosophila melanogaster*), and blowfly [63] (*Calliphora erythrocephala*) visual pigments. For housefly and blowfly, two distinct meta-states, M and M', were detected [61, 63]. For housefly, the relative fluorescence quantum yield of M and M' forms was also measured and the ratio $\Phi(M)/\Phi(M')$ was found to be >3. The authors suggested that M and M' meta-forms differ by *trans*- and *cis*- isomers of the 3-hydroxy-retinal, which serves as the chromophore in this species.

For bistable pigments, excited state lifetimes were measured for the octopus rhodopsin (*Paroctopus Delheini*) [60] and for the squid rhodopsin [54] and were found to be 0.14±0.07 ps and $0.12 \pm 0.05$ ps, respectively. As for the bovine rhodopsin, these values are lower than the lifetimes reported for microbial rhodopsins and the corresponding points are located in the bottom of Figure 4b.

In addition, it is worth paying some attention to studies that deal with photochemical properties of the protonated Schiff base other than fluorescence but that can be related to fluorescence efficiency. In a comprehensive spectroscopic study on photochemical



https://doi.org/10.26434/chemrxiv-2023-3n1d0 **ORCID:** https://orcid.org/0000-0003-3413-1706 Content not peer-reviewed by ChemRxiv. **License:** CC BY-NC-ND 4.0

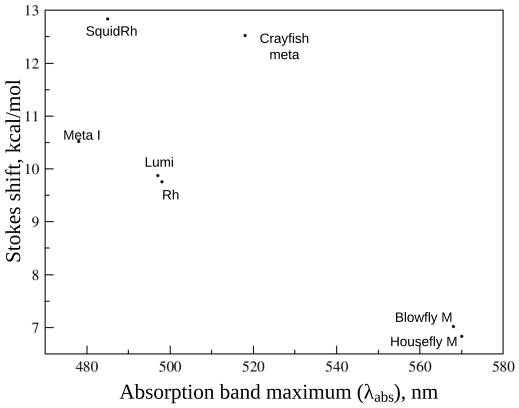


**Figure 5.** Stokes shifts (in kcal/mol) of animal rhodopsins and their photocycle intermediates as a function of $\lambda_{abs}$.

properties of the mouse melanopsin [64], a bistable non-visual animal opsin with 11-*cis* retinal in its most thermodynamically stable ground state ($\lambda_{abs} = 467$ nm) and all-*trans* retinal in meta-state ($\lambda_{abs} = 476$ nm), the photoisomerization quantum yield of ground state melanopsin was found to be more than twice larger than for metamelanopsin: $0.52 \pm 0.02$ and $0.22 \pm 0.01$, respectively. The photoisomerization quantum yield reported for the bovine visual rhodopsin ($0.65 \pm 0.01$ [65]) is closer to the photoisomerization quantum yield measured for the ground form of the mouse melanopsin than for the meta-form of this melanopsin.

Recent studies [66, 67] on photochemical properties of Rhodopsin-1 from the jumping spider *Hasarius adansoni* (JSR1), which possesses 11-*cis* retinal in its ground state ($\lambda_{abs} = 535$ nm) and all-*trans* retinal in meta state (Meta-JSR1) with a similar absorption band maximum ($\lambda_{abs} = 535$) nm but slightly bigger extinction coefficient [67], do not contain any information about fluorescence properties of either JSR1 or Meta-JSR1. However, simulations of photostationary state performed in Ref. [66] suggested lower quantum efficiencies for the reverse Meta-JSR1 $\rightarrow$ JSR1 transitions (0.4 - 0.5) than for the direct JSR1 $\rightarrow$ Meta-JSR1 transitions (0.7). These findings are again in line with the assumption that the photoisomerization process occurs more efficiently if a negative charge is present in the vicinity of $^{+}$N-H part of the retinal protonated Schiff base.

*Fluorescence emission and excitation band maxima and the Stokes shifts.* As is the case of microbial rhodopsins, the general trend of decreasing Stokes shifts at longer absorption band maxima wavelengths is observed for animal opsin-based photosensitive proteins. However, the available data are not sufficient to unambiguously derive any correlation (Figure 5).

## Retinal protonated Schiff based in the gas phase and solvents.

Recently, the excited state decay of the retinal protonated Schiff base (PSB) has been studied in the gas phase [68]. Due to extreme instability of the PSB in the gas phase, a special experimental approach combining time-resolved action spectroscopy with femtosecond pump-probe techniques in an ion-storage ring has been applied. The observed excited state decay was fitted by two components with $\approx 0.4$ ps and 3 ps lifetimes at room temperature and $\approx 1.4$ ps and 77 ps at 100 K. The fast and slow components were assigned to *cis* (most likely 11-*cis*) and all-*trans* forms of the chromophore, respectively. The temperature dependence was explained by potential energy barriers on the excited



https://doi.org/10.26434/chemrxiv-2023-3n1d0 **ORCID:** https://orcid.org/0000-0003-3413-1706 Content not peer-reviewed by ChemRxiv. **License:** CC BY-NC-ND 4.0

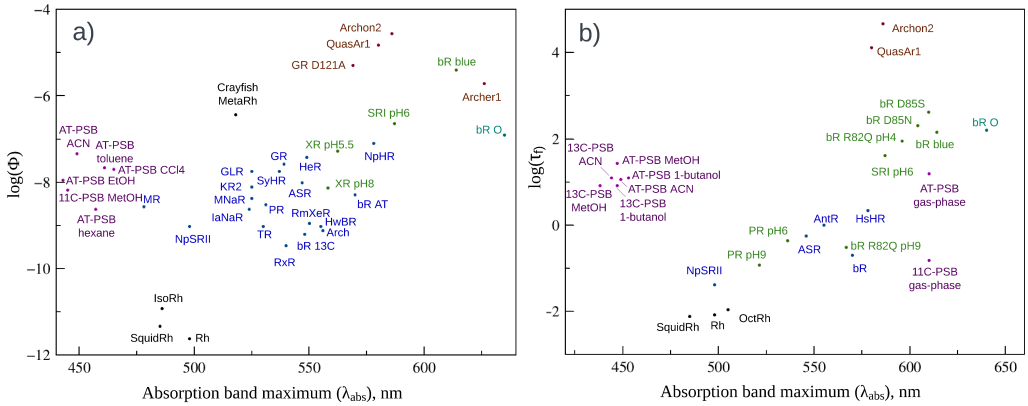


**Figure 6.** a) Fluorescence quantum yields logarithm (log Φ) of microbial, animal rhodopsins and retinal protonated Schiff base (PSB) isomers in solvents and gas phase as a function of absorption band maxima ($\lambda_{abs}$). b) Fluorescence lifetimes logarithm (log $\tau_f$) of microbial, animal rhodopsins and retinal PSB isomers in solvents and gas phase as a function of $\lambda_{abs}$. PSB isomers in solvents and gas phase are shown in purple. The color code for rhodopsins is defined as in Figure 4. For abbreviations of proteins, see Tables 1 and 2.

state potential energy surface that has to be overcome to achieve the conical intersection. This assumption was also supported by *ab initio* calculations.

The discussed combined experimental and computational study on PSB in the gas phase is of particular interest to rhodopsins photochemistry research since it provides the information about intrinsic photochemical properties of the chromophore in the absence of any interactions with protein or solvent environments. In Figure 6b, the points that represent the all-*trans* and 11-*cis* retinal PSB isomers in the gas phase are added to the previously discussed lifetimes of microbial and animal rhodopsins. Expectedly, the point corresponding to the all-*trans* isomer is located closer to the blue form of bacteriorhodopsin with the neutralized counterion than to the points of microbial rhodopsins at neutral pH; the point corresponding to the 11-*cis* chromophore also lies above the points corresponding to animal rhodopsins with deprotonated counterion but lower than the point of the all-*trans* isomer.

Finally, we considered studies on photoisomerization properties of the PSB (more precisely, of the PSB-counterion complexes) in different solvents. The data are compiled in Table 3 and Figure 6a,b. The points corresponding to the retinal PSB in different solvents are located at the left sides of Figures 6a,b since all chromophore isomers possess significantly blue-shifted absorption bands in solvents. Two patterns can be seen in Figures 6. Just as for rhodopsins and gas-phase PSBs, if data for the same solvent considered, the points corresponding to the 11-*cis* or 13-*cis* isomers lie below the points corresponding to the all-*trans* isomer. Fluorescence quantum yield of the all-*trans* isomer measured in a non-polar and low-polarizable solvent, hexane (Figure 6a), is lower than the quantum yield measured in polar or polarizable solvents. Apparently, in hexane shielding of the counterion may be lower than in polar and polarizable solvents but additional computational studies are required to test this assumption.

# Conclusion

Fluorescence and photoisomerization of the chromophore in opsin-based photosensitive proteins have been investigated for decades [7, 8, 69, 70]. Recently, the research in this



https://doi.org/10.26434/chemrxiv-2023-3n1d0 **ORCID:** https://orcid.org/0000-0003-3413-1706 Content not peer-reviewed by ChemRxiv. **License:** CC BY-NC-ND 4.0

area has been facilitated by application of rhodopsins as tools for optogenetics [71–73], which is, along with photopharmacology [74–77], a widely-used approach to control and monitor biological cell activity using light. Although high fluorescence and, accordingly, inefficient photoisomerization of the chromophore in rhodopsins is an impediment for application of these proteins as actuators, intense fluorescence is a desirable feature for their applications as genetically-encoded voltage indicators. For rational engineering of new variants of bright fluorescent rhodopsins, detailed understanding of how the protein environment tunes fluorescence properties is required. Besides, the knowledge of how a modification of protein composition or structure affects different fluorescence properties can be used to get a structural insight into rhodopsins and their photocycle intermediates based on fluorescence measurements.

The goal of this review is the compilation and analysis of available experimental data to identify and highlight main points that can be considered general for a variety of microbial and animal opsin-based photosensitive proteins. Vast majority of the available studies are performed for rhodopsins, i.e. opsins in which the retinal Schiff base serves as the cofactor. A few studies on visual pigments of the housefly, blowfly and Drosophila with the 3-hydroxy-retinal chromophore are also available and the data coincide well with the data for rhodopsins.

The all-*trans*-form of the chromophores of opsin-based photoactive proteins demonstrate slower excited state decay than the 11-*cis*-form in the gas phase. A similar trend is preserved for rhodopsins and the retinal PSB in solvents: fluorescence lifetime and fluorescence quantum yield is higher for rhodopsins with the all-*trans*-form of the retinal than for 11-*cis* or 13-*cis*-forms of the retinal PSB assuming that electrostatic environment is similar. A drastic change in fluorescence quantum yield and fluorescence lifetime is observed after transition to rhodopsins with neutralized counterion, i.e. to acidic forms, the O photocycle intermediate of microbial rhodopsins or meta-states of animal rhodopsins. Generally, one can conclude that the decrease of stabilization of a positive charge in the $^{+}$N-H part of the chromophore leads to enhanced fluorescence and slower excited state decay. In this context, the role of the counterion electrostatic effect is an important factor to achieve fluorescence enhancement. Analysis of the dependence of fluorescence efficiency on absorption band maxima reveals a clear trend of fluorescence enhancement with red-shifting of absorption bands but not a strong correlation. Surprisingly, a quite strong linear correlation ($R^2$= 0.86) exists between the Stokes shifts of microbial rhodopsins and absorption band maxima. Obviously, both the electrostatic and steric interactions of the chromophore with the protein environment can tune fluorescence properties. Although a counterion contribution to the electrostatic field in the chromophore region is decisive, the electrostatic effect of other charged and polar residues can also be significant. The steric interaction of the chromophore with surrounding residues of the binding pocket also can be an important factor for tuning the fluorescence properties. Further theoretical and experimental studies are needed to advance this subject.



https://doi.org/10.26434/chemrxiv-2023-3n1d0 **ORCID:** https://orcid.org/0000-0003-3413-1706 Content not peer-reviewed by ChemRxiv. **License:** CC BY-NC-ND 4.0

**Table 1.** Fluorescence properties of microbial rhodopsins. $\lambda_{abs}$ - absorption band maximum, $\lambda_{exc}$ - fluorescence excitation band maximum, $\lambda_{em}$ - emission band maximum, $\Phi$ - fluorescence quantum yield, $\tau_f$ - fluorescence lifetime. For biexponential decays, both $\tau_f$ values are given separated by a comma. Abbreviations: bR, *Halobacterium halobium* bacteriorhodopsin; AT, *all-trans* form; 13C, *13-cis* form; bR blue, blue form of bR at pH2.6; bR O and bR Q, O- and Q-intermediates of bR photocycle; Arch, archaerhodopsin-3; QuasAr1, Archon2, Archer1, bright mutants of archaerhodopsin-3; PR, proteorhodopsin from marine $\gamma$-proteobacteria; XR, xanthorhodopsin; GR, *Gloebacter violaceus* rhodopsin; ESR, *Exiguobacterium sibiricum* rhodopsin; HeR, heliorhodopsin.

| Protein | $\lambda_{abs}$, nm | $\lambda_{exc}$, nm | $\lambda_{em}$, nm | Stokes shift, nm | $\Phi$ | $\tau_f$, ps |
|---|---|---|---|---|---|---|
| bR | 568 [44, 78] | 570 [79] | 755 ± 10 [43] | 187 ± 10 | 2.5-2.7 $\cdot 10^{-4}$ (AT)<br>0.7-1.2 $\cdot 10^{-4}$ (13C)<br>[29] | 0.5 [78]<br>0.56 [31] |
| bR blue | 610-620 [80] | 613-614 [80] | 750 [29] | 130-140 | $4.5 \cdot 10^{-3}$ [80] | 1.5, 8.6 [81]<br>7.8 [31] |
| bR O | 635-640 [82] | - | 750 ± 5 [43] | 110-120 | $\approx 1 \cdot 10^{-3}$ [45] | 9 ± 2 [45] |
| bR Q | - | - | <720 [43] | - | $\Phi \approx 110 \cdot \Phi$(bR) [44]<br>$7 \cdot 10^{-3}$ [45] | 62 ± 2 [45] |
| bR D85S | 609 [83] | - | 760 [83] | 161 | - | 3.6, 14 [83] |
| bR D85N | 604 [38] | - | - | - | - | 2.0, 10 [38] |
| bR R82Q, pH4.4 | 596 [38] | - | - | - | - | 2.0, 7 [38] |
| bR R82Q, pH9.6 | 556 [38] | - | - | - | - | 0.6 [38] |
| Arch | 553 [23] | 553 [23] | 687 [23] | 134 | $1.1 \cdot 10^{-4}$ [23]<br>$9 \cdot 10^{-4}$ [84] | 5.9, 60 (intense illumination) [23] |
| Arch D95N | 585 [84] | - | 687 [84] | 102 | $4 \cdot 10^{-4}$ [84] | - |
| QuasAr1 | 580 [22, 85] | 590 [86]<br>585 [85] | 715 [86]<br>740 [85] | 135, 160 | $8 \cdot 10^{-3}$ [86]<br>$6.5 \cdot 10^{-3}$ [85] | 61.5 [85] |
| Archon2 | 586 [87] | - | 735 [87] | 149 | $1.05 \cdot 10^{-2}$ [87] | 106 [87] |
| Archer1 | 626 [88] | 627 [47] | 731 [88] | 103 | $3.3 \cdot 10^{-3}$ [88] | - |
| PR | 531 [89] | 565 [89] | 700 [89] | 169 | $2 \cdot 10^{-4}$ [89] | 1.4 [89]<br>0.7, 15 (pH6)<br>0.4, 8 (pH9) [35] |
| XR | 560 [33] | - | 685 [33] | 125 | $3 \cdot 10^{-4}$ (pH8)<br>$7 \cdot 10^{-4}$ (pH5.5)<br>[33] | - |
| GR | 541 [32] | 568 (pH4.5) [32]<br>550 [23] | 670 (pH7.2)<br>680 (pH4.5) [32]<br>723 [23] | 129 (pH7.2)<br>135 (pH4.5)<br>173 [23] | F(pH4.5)=<br>4F(pH7.2) [32]<br>$5.1 \cdot 10^{-4}$ [23] | 9.6, 47 (intense illumination) [23] |
| GR D121A | ≈ 568 [90] | - | - | - | $5 \cdot 10^{-3}$ [90] | - |
| ESR | 546 (pH2)<br>534 (pH5)<br>531 (pH7)<br>521 (pH10.5)<br>[34] | 565 (pH5)<br>556 (pH7)<br>538 (pH8.8)<br>[34] | ≈ 690 [34] | ≈ 159 | F(pH5) =<br>2F(pH7)<br>[34] | - |
| ESR D85N | 563 (pH5)<br>[34] | 564(pH5)<br>[34] | 686 [34] | 123 | F=7F(ESR)<br>[34] | - |
| ESR H57M | 565 (pH5)<br>517 (pH8.5)<br>[34] | 568 (pH4.5)<br>520 (pH8.8)<br>[34] | 690 (pH4.5)<br>650 (pH7.5)<br>[34] | 125 (pH4.5)<br>133 (pH8) | F(pH4.5)≈<br>100F(pH9)<br>[34] | - |
| HeR | 549 [91] | - | ≈700 [91] | 151 | $6 \cdot 10^{-4}$ [91] | - |



https://doi.org/10.26434/chemrxiv-2023-3n1d0 **ORCID:** https://orcid.org/0000-0003-3413-1706 Content not peer-reviewed by ChemRxiv. **License:** CC BY-NC-ND 4.0

**Table 1 (continuation).** Fluorescence properties of microbial rhodopsins. $\lambda_{abs}$ - absorption band maximum, $\lambda_{exc}$ - fluorescence excitation band maximum, $\lambda_{em}$ - emission band maximum, $\Phi$ - fluorescence quantum yield, $\tau_f$ - fluorescence lifetime; (int) - fluorescence lifetimes detected under intense illumination. Abbreviations: ASR, Anabaena sensory rhodopsin; KR2, Krokinobacter rhodopsin 2 from *Krokinobacter eikastus*; RxR, rhodopsin from *Rubrobacter xylanophilus*; NpHR, halorhodopsin from *Natronomonas pharaonis*; GLR, sodium pumping rhodopsin from *Gillisia limnaea*; HwBR, bacteriorhodopsin from *Haloquadratum walsbyi*; IaNaR, sodium pumping rhodopsin from *Indibacter alkaliphilus*; MNaR, sodium pumping rhodopsin from *Micromonospora* sp. CNB394; MR, middle rhodopsin from *Haloquadratum walsbyi*; HsHR, halorhodopsin from *Halobacterium salinarum*; SRII, sensory rhodopsin II from *Natronobacterium pharaonis*; SRI, sensory rhoodopsin I from *Halobacterium salinarum*; RmXer, xenorhodopsin from *Rubricoccus marinus*; SyHR, Synechocystis halorhodopsin from *Synechocystis* sp. PCC 7509; TR, thermophilic rhodopsin from *Thermus thermophilus* JL-18; AntR, antarctic rhodopsin.

| Protein | $\lambda_{abs}$, nm | $\lambda_{exc}$, nm | $\lambda_{em}$, nm | Stokes shift, nm | $\Phi$ | $\tau_f$, ps |
|---|---|---|---|---|---|---|
| ASR | 541 (pH7) [23]<br>547 (AT) [92]<br>533 (13C) [92] | 540 (pH7) [23] | 700 [23] | 160 | $3.3 \cdot 10^{-4}$ (AT)<br>$0.8 \cdot 10^{-4}$<br>(13C) [93] | 0.1, 0.77 [94] |
| KR2 | 525 [23] | 525 [23] | 685 [23] | 160 | $3 \cdot 10^{-4}$ [23] | 8.2, 46<br>(intense<br>illumination)<br>[23] |
| RxR | 540 [23] | 540 [23] | 708 [23] | 168 | $0.77 \cdot 10^{-4}$ [23] | 5.2, 54<br>(intense<br>illumination)<br>[23] |
| NpHR | 576 [23] | 576 [23] | 715 [23, 95]<br>$\approx$ 750 [96] | 115<br>150 | $8.3 \cdot 10^{-4}$ [23]<br>$5 \cdot 10^{-4}$ [96] | 6.7, 24<br>(intense<br>illumination)<br>[23]<br>0.17, 1.5,<br>8.5 [97]<br>2.3 [95] |
| GLR | 525 [23] | 520 [23] | 685 [23] | 165 | $4.3 \cdot 10^{-4}$ [23] | - |
| HwBR | 555 [23] | 550 [23] | 720 [23] | 170 [23] | $1.2 \cdot 10^{-4}$ [23] | - |
| IaNaR | 524 [23] | 525 [23] | 690 [23] | 165 [23] | $1.8 \cdot 10^{-4}$ [23] | - |
| MNaR | 525 [23] | 500 [23] | 665 [23] | 165 [23] | $2.3 \cdot 10^{-4}$ [23] | - |
| MR | 478 [23] | 460 [23] | 620 [23] | 160 [23] | $1.9 \cdot 10^{-4}$ [23] | - |
| HsHR | 578 [97] | - | - | - | - | 1.5. 8.5 [97] |
| NpSRII | 498 [23, 95]<br>460 [95] | 460 [23] | 615 [23]<br>630 [95] | 155 [23]<br>132 [95] | $1.2 \cdot 10^{-4}$ [23, 98] | 0.25, 3.0 [95] |
| SRI pH6 | 587 [98] | - | 700 [98] | 113 | $\approx 1.3 \cdot 10^{-3}$ [98] | 5, 33 [98] |
| RmXeR | 550 [23] | 545 [23] | 715 [23] | 170 [23] | $1.3 \cdot 10^{-4}$ [23] | - |
| SyHR | 537 [23] | 535 [23] | 680 [23] | 145 [23] | $4.3 \cdot 10^{-4}$ [23] | - |
| TR | 530 [23] | 518 [23] | 680 [23] | 162 [23] | $1.2 \cdot 10^{-4}$ [23] | - |
| AntR | 555 [99] | - | - | - | - | 1, 5 [99] |
| NeoR | 690 [10] | - | 707 [10] | 17 | 0.2 [10] | 1100 [10] |



https://doi.org/10.26434/chemrxiv-2023-3n1d0 **ORCID:** https://orcid.org/0000-0003-3413-1706 Content not peer-reviewed by ChemRxiv. **License:** CC BY-NC-ND 4.0

**Table 2.** Fluorescence properties of animal rhodopsins. $\lambda_{abs}$ - absorption band maximum, $\lambda_{exc}$ - fluorescence excitation band maximum, $\lambda_{em}$ - emission band maximum, $\Phi$ - fluorescence quantum yield, $\tau_f$ - fluorescence lifetime. Abbreviations: Rh, bovine (*Bos Taurus*) rhodopsin; IsoRh, bovine isorhodopsin; SquidRh, squid (*Todarodes Pacificus*) rhodopsin; OctRh, octopus (*Paroctopus Defleini*) rhodopsin; Batho, bovine bathorhodopsin; Lumi, bovine lumirhodopsin; MetaI and MetaII, bovine metarhodopsins I and II; Crayfish meta, metarhodopsin from crayfish *Orconectes rusticus*; Blowfly meta, metaxanthopsin from blowfly *Calliphora erythrocephala*; Housefly meta, metaxanthopsin from housefly *Musca domestica*; Droso meta, metaxanthopsin from *Drosophila melanogaster*.

| Protein | $\lambda_{abs}$, nm | $\lambda_{exc}$, nm | $\lambda_{em}$, nm | Stokes shift, nm | $\Phi$ | $\tau_f$, ps |
|---|---|---|---|---|---|---|
| Rh | 498 [54] | - | 600 [54] | 102 | $1.2 \cdot 10^{-5}$ [54]<br>$0.9 \cdot 10^{-5}$ [56] | 0.05 [56]<br>0.146, 1.5 [53]<br>0.125, 1 [100] |
| IsoRh | 485 [56] | - | $\approx$ 620 [56] | 135 | $1.8 \cdot 10^{-5}$ [56] | - |
| SquidRh | 485 [54] | - | 620 [54] | 135 | $1.2 \cdot 10^{-5}$ [54] | 0.12 [54] |
| OctRh | 505 [60] | - | - | - | - | 0.14 [60] |
| Batho | 543 [101] | - | - | - | $< 10^{-5}$ [101] | - |
| Lumi | 497 [55] | - | 600 | 103 | $< 10^{-5}$ [55] | - |
| MetaI | 478 [55] | - | 580 | 102 | $< 10^{-5}$ [55] | - |
| MetaII | 380 [55] | - | 500-515 | 120 | $< 10^{-5}$ [55] | - |
| Crayfish meta | - | 518 [59] | 660-670 [59] | 142 | $1.6 \cdot 10^{-3}$ [59] | - |
| Blowfly meta | 584 (M)<br>568 (M') [63] | - | 660 [63] | 92 | $\Phi$(M')><br>3$\Phi$(M) [63] | - |
| Housefly meta | 580 (M)<br>570 (M') [61] | - | 660 [61] | 90 | - | - |
| Droso meta | - | 570 [62] | >646 [62] | - | - | - |



https://doi.org/10.26434/chemrxiv-2023-3n1d0 **ORCID:** https://orcid.org/0000-0003-3413-1706 Content not peer-reviewed by ChemRxiv. **License:** CC BY-NC-ND 4.0

**Table 3.** Fluorescence properties of retinal in the gas-phase and solvents. $\lambda_{abs}$ - absorption band maximum, $\lambda_{exc}$ - fluorescence excitation band maximum, $\lambda_{em}$ - emission band maximum, $\Phi$ - fluorescence quantum yield, $\tau_f$ - fluorescence lifetime. Abbreviations: AT-PSB, 13C, and 11C-PSB - all-*trans*, 13-*cis*, and 11-*cis* retinal protonated Schiff base. Numbers in parenthesis denote illumination wavelength.

| Species | Solvent | $\lambda_{abs}$, nm | $\lambda_{em}$, nm | Stokes shift, nm | $\Phi$ | $\tau_F$ |
|---|---|---|---|---|---|---|
| 11C-PSB | gas-phase | 610 [68] | - | - | - | 0.442 ± 0.121 ps [68,102] |
| AT-PSB | gas-phase | 610 [68] | - | - | - | 3.3 ± 1 ps [68] |
| AT-PSB | methanol | 445 [103]<br>442 [104]<br>447 [105] | 655 [103]<br>675 [104]<br>630 [105] | 210 [103]<br>233 [104]<br>183 [105] | - | 90 fs (525)<br>0.5, 2.8 ps (605)<br>3.7 ps (762) [103]<br><0.2, 4.2 ps [105] |
| 13C-PSB | methanol | 438 [105] | 630 [105] | 192 | - | 2.5 ps |
| 11C-PSB | methanol | 445 [106] | 660 [106] | 215 | $2.8 \cdot 10^{-4}$ [106] | 0.5, 2.0 ps (605)<br>3.1 ps (695) [106] |
| AT-PSB | acetonitrile | 449 [105] | 690 [104]<br>650 [105] | 241<br>201 | $6.5 \cdot 10^{-4}$ [104] | <5 ps [104]<br>2.9 ps [105] |
| 13C-PSB | acetonitrile | 444 [105] | 652 [105] | 208 | - | 3.0 ps [105] |
| AT-PSB | 1-butanol | 453 [105] | 610 [105] | 157 | - | 3.0 ps [105] |
| 13C-PSB | 1-butanol | 447 [105] | 603 [105] | 156 | - | 2.5 ps [105] |
| AT-PSB | hexane | 457 [104] | 620 [104] | 163 | $1.8 \cdot 10^{-4}$ [104] | <5 ps [104] |
| AT-PSB | carbon tetrachloride | 465 [104] | 650 [104] | 185 | $4.5 \cdot 10^{-4}$ [104] | - |
| AT-PSB | toluene | 461 [104] | 660 [104] | 199 | $4.7 \cdot 10^{-4}$ [104] | - |
| AT-PSB | ethyl acetate | 432 [104] | 650 [104] | 218 | - | - |
| AT-PSB | acetone | 447 [104] | 680 [104] | 233 | - | - |
| AT-PSB | ethanol | 443 [104] | 660 [104] | 217 | $3.5 \cdot 10^{-4}$ [104] | <6 ps [104] |
| AT-PSB | propanol | 449 [104] | 650 [104] | 201 | - | - |


## Acknowledgments

The study was funded by the Russian Science Foundation (RSF), grant No. 23-73-00041. The research is carried out using the equipment of the shared research facilities of HPC computing resources at Lomonosov Moscow State University. The authors also acknowledge computational resources of Peter the Great Saint Petersburg Polytechnic University Supercomputing Center (www.spbstu.ru). Dedicated to the 300th anniversary of Saint Petersburg State University.




https://doi.org/10.26434/chemrxiv-2023-3n1d0 **ORCID:** https://orcid.org/0000-0003-3413-1706 Content not peer-reviewed by ChemRxiv. **License:** CC BY-NC-ND 4.0

## References


1. Takashi Nagata and Keiichi Inoue. Rhodopsins at a glance. *J. Cell Sci.*, 134(22):jcs258989, 2021.

2. Andrey Rozenberg, Keiichi Inoue, Hideki Kandori, and Oded Béjà. Microbial rhodopsins: the last two decades. *Annu. Rev. Microbiol.*, 75:427–447, 2021.

3. Dmitry Bratanov, Kirill Kovalev, Jan-Philipp Machtens, Roman Astashkin, Igor Chizhov, Dmytro Soloviov, Dmytro Volkov, Vitaly Polovinkin, Dmitrii Zabelskii, Thomas Mager, et al. Unique structure and function of viral rhodopsins. *Nat. Commun.*, 10(1):4939, 2019.

4. Sarah M Andrew, Carly M Moreno, Kaylie Plumb, Babak Hassanzadeh, Laura Gomez-Consarnau, Stephanie N Smith, Oscar Schofield, Susumu Yoshizawa, Takayoshi Fujiwara, William G Sunda, et al. Widespread use of proton-pumping rhodopsin in antarctic phytoplankton. *Proc. Natl. Acad. Sci. U.S.A.*, 120(39):e2307638120, 2023.

5. Keiichi Inoue. Diversity, mechanism, and optogenetic application of light-driven ion pump rhodopsins. *Optogenetics: Light-Sensing Proteins and Their Applications in Neuroscience and Beyond*, pages 89–126, 2021.

6. Willem J de Grip and Srividya Ganapathy. Rhodopsins: an excitingly versatile protein species for research, development and creative engineering. *Front. Chem.*, 10:879609, 2022.

7. Keiichi Inoue. Photochemistry of the retinal chromophore in microbial rhodopsins. *J. Phys. Chem. B*, 2023.

8. Mikhail A Ostrovsky, Olga A Smitienko, Anastasia V Bochenkova, and Tatiana B Feldman. Similarities and differences in photochemistry of type i and type ii rhodopsins. *Biochemistry*, 88(10):1528–1543, 2023.

9. Masato Sumita, Mikhail N Ryazantsev, and Kazuya Saito. Acceleration of the z to e photoisomerization of penta-2, 4-dieniminium by hydrogen out-of-plane motion: theoretical study on a model system of retinal protonated schiff base. *Phys. Chem. Chem. Phys.*, 11(30):6406–6414, 2009.

10. Masahiro Sugiura, Kazuki Ishikawa, Kota Katayama, Yuji Sumii, Rei Abe-Yoshizumi, Satoshi P Tsunoda, Yuji Furutani, Norio Shibata, Leonid S Brown, and Hideki Kandori. Unusual photoisomerization pathway in a near-infrared light absorbing enzymerhodopsin. *J. Phys. Chem. Lett.*, 13(40):9539–9543, 2022.

11. Matthias Broser. Far-red absorbing rhodopsins, insights from heterodimeric rhodopsin-cyclases. *Front. Mol. Biosci.*, 8:806922, 2022.

12. Matthias Broser, Wayne Busse, Anika Spreen, Maila Reh, Yinth Andrea Bernal Sierra, Songhwan Hwang, Tillmann Utesch, Han Sun, and Peter Hegemann. Diversity of rhodopsin cyclases in zoospore-forming fungi. *Proc. Natl. Acad. Sci. U.S.A.*, 120(44):e2310600120, 2023.

13. Linlin Z Fan, Doo Kyung Kim, Joshua H Jennings, He Tian, Peter Y Wang, Charu Ramakrishnan, Sawyer Randles, Yanjun Sun, Elina Thadhani, Yoon Seok Kim, et al. All-optical physiology resolves a synaptic basis for behavioral timescale plasticity. *Cell*, 186(3):543–559, 2023.




https://doi.org/10.26434/chemrxiv-2023-3n1d0 **ORCID:** https://orcid.org/0000-0003-3413-1706 Content not peer-reviewed by ChemRxiv. **License:** CC BY-NC-ND 4.0

14. Miao-Ping Chien, Daan Brinks, Guilherme Testa-Silva, He Tian, F Phil Brooks III, Yoav Adam, Blox Bloxham, Benjamin Gmeiner, Simon Kheifets, and Adam E Cohen. Photoactivated voltage imaging in tissue with an archaerhodopsin-derived reporter. *Sci. Adv.*, 7(19):eabe3216, 2021.

15. Kiryl D Piatkevich and Edward S Boyden. Optogenetic control of neural activity: the biophysics of microbial rhodopsins in neuroscience. *Q. Rev. Biophys.*, pages 1–81, 2023.

16. Moritz Armbruster, Saptarnab Naskar, Jacqueline P Garcia, Mary Sommer, Elliot Kim, Yoav Adam, Philip G Haydon, Edward S Boyden, Adam E Cohen, and Chris G Dulla. Neuronal activity drives pathway-specific depolarization of peripheral astrocyte processes. *Nat. Neurosci.*, 25(5):607–616, 2022.

17. Kiryl D Piatkevich, Seth Bensussen, Hua-an Tseng, Sanaya N Shroff, Violeta Gisselle Lopez-Huerta, Demian Park, Erica E Jung, Or A Shemesh, Christoph Straub, Howard J Gritton, et al. Population imaging of neural activity in awake behaving mice. *Nature*, 574(7778):413–417, 2019.

18. Laurent C Moreaux, Dimitri Yatsenko, Wesley D Sacher, Jaebin Choi, Changhyuk Lee, Nicole J Kubat, R James Cotton, Edward S Boyden, Michael Z Lin, Lin Tian, et al. Integrated neurophotonics: toward dense volumetric interrogation of brain circuit activity—at depth and in real time. *Neuron*, 108(1):66–92, 2020.

19. Xiao Min Zhang, Tatsushi Yokoyama, and Masayuki Sakamoto. Imaging voltage with microbial rhodopsins. *Front. Mol. Biosci.*, 8:738829, 2021.

20. Dmitrii M Nikolaev, Vladimir N Mironov, Andrey A Shtyrov, Iaroslav D Kvashnin, Andrey S Mereshchenko, Andrey V Vasin, Maxim S Panov, and Mikhail N Ryazantsev. Fluorescence imaging of cell membrane potential: From relative changes to absolute values. *Int. J. Mol. Sci.*, 24(3):2435, 2023.

21. Xin Meng, Srividya Ganapathy, Lars van Roemburg, Marco Post, and Daan Brinks. Voltage imaging with engineered proton-pumping rhodopsins: Insights from the proton transfer pathway. *ACS Phys. Chem. Au*, 3(4):320–333, 2023.

22. Arita Silapetere, Songhwan Hwang, Yusaku Hontani, Rodrigo G Fernandez Lahore, Jens Balke, Francisco Velazquez Escobar, Martijn Tros, Patrick E Konold, Rainer Matis, Roberta Croce, et al. Quasar odyssey: the origin of fluorescence and its voltage sensitivity in microbial rhodopsins. *Nat. Commun.*, 13(1):5501, 2022.

23. Keiichi Kojima, Rika Kurihara, Masayuki Sakamoto, Tsukasa Takanashi, Hikaru Kuramochi, Xiao Min Zhang, Haruhiko Bito, Tahei Tahara, and Yuki Sudo. Comparative studies of the fluorescence properties of microbial rhodopsins: spontaneous emission versus photointermediate fluorescence. *J. Phys. Chem. B*, 124(34):7361–7367, 2020.

24. Kazuhiro J Fujimoto. Electronic couplings and electrostatic interactions behind the light absorption of retinal proteins. *Front. Mol. Biosci.*, 8:752700, 2021.

25. Masaki Tsujimura and Hiroshi Ishikita. Insights into the protein functions and absorption wavelengths of microbial rhodopsins. *J. Phys. Chem. B*, 124(52):11819–11826, 2020.

26. Se-Hwan Kim, Kimleng Chuon, Shin-Gyu Cho, Ahreum Choi, Seanghun Meas, Hyun-Suk Cho, and Kwang-Hwan Jung. Color-tuning of natural variants of heliorhodopsin. *Sci. Rep.*, 11(1):854, 2021.



https://doi.org/10.26434/chemrxiv-2023-3n1d0 **ORCID:** https://orcid.org/0000-0003-3413-1706 Content not peer-reviewed by ChemRxiv. **License:** CC BY-NC-ND 4.0

27. Andrey A Shtyrov, Dmitrii M Nikolaev, Vladimir N Mironov, Andrey V Vasin, Maxim S Panov, Yuri S Tveryanovich, and Mikhail N Ryazantsev. Simple models to study spectral properties of microbial and animal rhodopsins: Evaluation of the electrostatic effect of charged and polar residues on the first absorption band maxima. *Int. J. Mol. Sci.*, 22(6):3029, 2021.

28. Mikhail N Ryazantsev, Ahmet Altun, and Keiji Morokuma. Color tuning in rhodopsins: the origin of the spectral shift between the chloride-bound and anion-free forms of halorhodopsin. *J. Am. Chem. Soc.*, 134(12):5520–5523, 2012.

29. T Kouyama, K Kinosita, and A Ikegami. Excited-state dynamics of bacteriorhodopsin. *Biophys. J.*, 47(1):43–54, 1985.

30. LS Brown, L Bonet, R Needleman, and JK Lanyi. Estimated acid dissociation constants of the schiff base, asp-85, and arg-82 during the bacteriorhodopsin photocycle. *Biophys. J.*, 65(1):124–130, 1993.

31. Chun-Fu Chang, Hikaru Kuramochi, Manish Singh, Rei Abe-Yoshizumi, Tatsuya Tsukuda, Hideki Kandori, and Tahei Tahara. A unified view on varied ultrafast dynamics of the primary process in microbial rhodopsins. *Angew. Chem. Int. Ed.*, 61(2):e202111930, 2022.

32. Eleonora S Imasheva, Sergei P Balashov, Ah Reum Choi, Kwang-Hwan Jung, and Janos K Lanyi. Reconstitution of gloeobacter violaceus rhodopsin with a light-harvesting carotenoid antenna. *Biochemistry*, 48(46):10948–10955, 2009.

33. Sergei P Balashov, Eleonora S Imasheva, Jennifer M Wang, and Janos K Lanyi. Excitation energy-transfer and the relative orientation of retinal and carotenoid in xanthorhodopsin. *Biophys. J.*, 95(5):2402–2414, 2008.

34. SP Balashov, LE Petrovskaya, EP Lukashev, ES Imasheva, AK Dioumaev, JM Wang, SV Sychev, DA Dolgikh, AB Rubin, MP Kirpichnikov, et al. Aspartate–histidine interaction in the retinal schiff base counterion of the light-driven proton pump of exiguobacterium sibiricum. *Biochemistry*, 51(29):5748–5762, 2012.

35. Robert Huber, Thomas Köhler, Martin O Lenz, Ernst Bamberg, Rolf Kalmbach, Martin Engelhard, and Josef Wachtveitl. ph-dependent photoisomerization of retinal in proteorhodopsin. *Biochemistry*, 44(6):1800–1806, 2005.

36. Chun-Fu Chang, Hikaru Kuramochi, Manish Singh, Rei Abe-Yoshizumi, Tatsuya Tsukuda, Hideki Kandori, and Tahei Tahara. Acid–base equilibrium of the chromophore counterion results in distinct photoisomerization reactivity in the primary event of proteorhodopsin. *Phys. Chem. Chem. Phys.*, 21(46):25728–25734, 2019.

37. Shinya Tahara, Satoshi Takeuchi, Rei Abe-Yoshizumi, Keiichi Inoue, Hiroyuki Ohtani, Hideki Kandori, and Tahei Tahara. Origin of the reactive and nonreactive excited states in the primary reaction of rhodopsins: ph dependence of femtosecond absorption of light-driven sodium ion pump rhodopsin kr2. *J. Phys. Chem. B*, 122(18):4784–4792, 2018.

38. Li Song, MA El-Sayed, and JK Lanyi. Protein catalysis of the retinal subpicosecond photoisomerization in the primary process of bacteriorhodopsin photosynthesis. *Science*, 261(5123):891–894, 1993.

39. Keiichi Kojima and Yuki Sudo. Convergent evolution of animal and microbial rhodopsins. *RSC Adv.*, 13(8):5367–5381, 2023.



https://doi.org/10.26434/chemrxiv-2023-3n1d0 **ORCID:** https://orcid.org/0000-0003-3413-1706 Content not peer-reviewed by ChemRxiv. **License:** CC BY-NC-ND 4.0

40. Oliver P Ernst, David T Lodowski, Marcus Elstner, Peter Hegemann, Leonid S Brown, and Hideki Kandori. Microbial and animal rhodopsins: structures, functions, and molecular mechanisms. *Chem. Rev.*, 114(1):126–163, 2014.

41. Denis Maag, Thilo Mast, Marcus Elstner, Qiang Cui, and Tomáš Kubař. O to br transition in bacteriorhodopsin occurs through a proton hole mechanism. *Proc. Natl. Acad. Sci. U.S.A.*, 118(39):e2024803118, 2021.

42. Sergei P Balashov, Eleonora S Imasheva, Rajni Govindjee, and Thomas G Ebrey. Titration of aspartate-85 in bacteriorhodopsin: what it says about chromophore isomerization and proton release. *Biophys. J.*, 70(1):473–481, 1996.

43. Hiroyuki Ohtani, Yasuhisa Tsukamoto, Yuusaku Sakoda, and Hiro-o Hamaguchi. Fluorescence spectra of bacteriorhodopsin and the intermediates o and q at room temperature. *FEBS Lett.*, 359(1):65–68, 1995.

44. Narutoshi Kamiya, Mitsuru Ishikawa, Kaname Kasahara, Manabu Kaneko, Noritaka Yamamoto, and Hiroyuki Ohtani. Picosecond fluorescence spectroscopy of the purple membrane of halobacterium halobium in alkaline suspension. *Chem. Phys. Lett.*, 265(6):595–599, 1997.

45. Hiroyuki Ohtani, Manabu Kaneko, Mitsuru Ishikawa, Narutoshi Kamiya, and Noritaka Yamamoto. Picosecond-millisecond dual-time-base spectroscopy of fluorescent photointermediates formed in the purple membrane of halobacterium halobium. *Chem. Phys. Lett.*, 299(6):571–575, 1999.

46. Dougal Maclaurin, Veena Venkatachalam, Hohjai Lee, and Adam E Cohen. Mechanism of voltage-sensitive fluorescence in a microbial rhodopsin. *Proc. Natl. Acad. Sci. U.S.A.*, 110(15):5939–5944, 2013.

47. Dmitrii M Nikolaev, Vladimir N Mironov, Ekaterina M Metelkina, Andrey A Shtyrov, Andrey S Mereshchenko, Nikita A Demidov, Svetlana E Moskalenko, Stanislav A Bondarev, Galina A Zhouravleva, Andrey V Vasin, Maxim S Panov, and Mikhail N Ryazantsev. Rational design of far-red archaerhodopsin3-based fluorescent genetically-encoded voltage indicators: from elucidation of fluorescence mechanism in archers to novel red-shifted variants. *Submitted to ACS Phys. Chem. Au.*

48. Dmitrii M Nikolaev, Andrey A Shtyrov, Andrey S Mereshchenko, Maxim S Panov, Yuri S Tveryanovich, and Mikhail N Ryazantsev. An assessment of water placement algorithms in quantum mechanics/molecular mechanics modeling: The case of rhodopsins' first spectral absorption band maxima. *Phys. Chem. Chem. Phys.*, 22(32):18114–18123, 2020.

49. Dmitrii M Nikolaev, Andrey A Shtyrov, Maxim S Panov, Adeel Jamal, Oleg B Chakchir, Vladimir A Kochemirovsky, Massimo Olivucci, and Mikhail N Ryazantsev. A comparative study of modern homology modeling algorithms for rhodopsin structure prediction. *ACS omega*, 3(7):7555–7566, 2018.

50. Wei-Wu Wang, Oleg A Sineshchekov, Elena N Spudich, and John L Spudich. Spectroscopic and photochemical characterization of a deep ocean proteorhodopsin. *J. Bio. Chem.*, 278(36):33985–33991, 2003.

51. Yamit Sharaabi, Vlad Brumfeld, and Mordechai Sheves. Binding of anions to proteorhodopsin affects the asp97 p k a. *Biochemistry*, 49(21):4457–4465, 2010.



https://doi.org/10.26434/chemrxiv-2023-3n1d0 **ORCID:** https://orcid.org/0000-0003-3413-1706 Content not peer-reviewed by ChemRxiv. **License:** CC BY-NC-ND 4.0

52. Steven O Smith. Mechanism of activation of the visual receptor rhodopsin. *Annu. Rev. Biophys.*, 52:301–317, 2023.

53. Haik Chosrowjan, Noboru Mataga, Yutaka Shibata, Shuji Tachibanaki, Hideki Kandori, Yoshinori Shichida, Tetsuji Okada, and Tsutomu Kouyama. Rhodopsin emission in real time: a new aspect of the primary event in vision. *J. Am. Chem. Soc.*, 120(37):9706–9707, 1998.

54. AG Doukas, MR Junnarkar, RR Alfano, RH Callender, Toshiaki Kakitani, and Barry Honig. Fluorescence quantum yield of visual pigments: evidence for subpicosecond isomerization rates. *Proc. Natl. Acad. Sci. U.S.A.*, 81(15):4790–4794, 1984.

55. AV Guzzo and GL Pool. Fluorescence spectra of the intermediates of rhodopsin bleaching. *Photochem. Photobiol.*, 9(6):565–570, 1969.

56. Gerd G Kochendoerfer and Richard A Mathies. Spontaneous emission study of the femtosecond isomerization dynamics of rhodopsin. *J. Phys. Chem.*, 100(34):14526–14532, 1996.

57. Takahiro Yamashita. Unexpected molecular diversity of vertebrate nonvisual opsin opn5. *Biophys. Rev.*, 12(2):333–338, 2020.

58. Mitsumasa Koyanagi, Tomoka Saito, Seiji Wada, Takashi Nagata, Emi Kawano-Yamashita, and Akihisa Terakita. Optogenetic potentials of diverse animal opsins: parapinopsin, peropsin, lws bistable opsin. *Optogenetics: Light-Sensing Proteins and Their Applications in Neuroscience and Beyond*, pages 141–151, 2021.

59. TW Cronin and TH Goldsmith. Fluorescence of crayfish metarhodopsin studied in single rhabdoms. *Biophys. J.*, 35(3):653–664, 1981.

60. Takayoshi Kobayashi, Mijong Kim, Makoto Taiji, Tatsuo Iwasa, Masashi Nakagawa, and Motoyuki Tsuda. Femtosecond spectroscopy of halorhodopsin and rhodopsin in a broad spectral range of 400- 1000 nm. *J. Phys. Chem. B*, 102(1):272–280, 1998.

61. DG Stavenga, N Franceschini, and K Kirschfeld. Fluorescence of housefly visual pigment. *Photochem. Photobiol.*, 40(5):653–659, 1984.

62. GV Miller, KA Itoku, AB Fleischer, and WS Stark. Studies of fluorescence in drosophila compound eyes: changes induced by intense light and vitamin a deprivation. *J. Comp. Physiol. A*, 154:297–305, 1984.

63. B Kruizinga and DG Stavenga. Fluorescence spectra of blowfly metaxanthopsins. *Photochem. Photobiol.*, 51(2):197–201, 1990.

64. Take Matsuyama, Takahiro Yamashita, Yasushi Imamoto, and Yoshinori Shichida. Photochemical properties of mammalian melanopsin. *Biochemistry*, 51(27):5454–5462, 2012.

65. Judy E Kim, Michael J Tauber, and Richard A Mathies. Wavelength dependent cis-trans isomerization in vision. *Biochemistry*, 40(46):13774–13778, 2001.

66. David Ehrenberg, Niranjan Varma, Xavier Deupi, Mitsumasa Koyanagi, Akihisa Terakita, Gebhard FX Schertler, Joachim Heberle, and Elena Lesca. The two-photon reversible reaction of the bistable jumping spider rhodopsin-1. *Biophys. J.*, 116(7):1248–1258, 2019.



https://doi.org/10.26434/chemrxiv-2023-3n1d0 **ORCID:** https://orcid.org/0000-0003-3413-1706 Content not peer-reviewed by ChemRxiv. **License:** CC BY-NC-ND 4.0

67. Niranjan Varma, Eshita Mutt, Jonas Mühle, Valérie Panneels, Akihisa Terakita, Xavier Deupi, Przemyslaw Nogly, Gebhard FX Schertler, and Elena Lesca. Crystal structure of jumping spider rhodopsin-1 as a light sensitive gpcr. *Proc. Natl. Acad. Sci. U.S.A.*, 116(29):14547–14556, 2019.

68. Hjalte V Kiefer, Elisabeth Gruber, Jeppe Langeland, Pavel A Kusochek, Anastasia V Bochenkova, and Lars H Andersen. Intrinsic photoisomerization dynamics of protonated schiff-base retinal. *Nat. Commun.*, 10(1):1210, 2019.

69. Shinya Tahara, Manish Singh, Hikaru Kuramochi, Wataru Shihoya, Keiichi Inoue, Osamu Nureki, Oded Béjà, Yasuhisa Mizutani, Hideki Kandori, and Tahei Tahara. Ultrafast dynamics of heliorhodopsins. *J. Phys. Chem. B*, 123(11):2507–2512, 2019.

70. Mikhail N Ryazantsev, Dmitrii M Nikolaev, Andrey V Struts, and Michael F Brown. Quantum mechanical and molecular mechanics modeling of membrane-embedded rhodopsins. *J. Membr. Biol.*, 252:425–449, 2019.

71. Valentina Emiliani, Emilia Entcheva, Rainer Hedrich, Peter Hegemann, Kai R Konrad, Christian Lüscher, Mathias Mahn, Zhuo-Hua Pan, Ruth R Sims, Johannes Vierock, et al. Optogenetics for light control of biological systems. *Nat. Rev. Methods Primers*, 2(1):55, 2022.

72. Wenqing Chen, Chen Li, Wanmin Liang, Yunqi Li, Zhuoheng Zou, Yunxuan Xie, Yangzeng Liao, Lin Yu, Qianyi Lin, Meiying Huang, et al. The roles of optogenetics and technology in neurobiology: a review. *Front. Aging Neurosci.*, 14:867863, 2022.

73. Dmitrii M Nikolaev, Maxim S Panov, Andrey A Shtyrov, Vitaly M Boitsov, Sergey Yu Vyazmin, Oleg B Chakchir, Igor P Yakovlev, and Mikhail N Ryazantsev. Perspective tools for optogenetics and photopharmacology: From design to implementation. *Progress in Photon Science: Recent Advances*, pages 139–172, 2019.

74. PD Bregestovski and GV Maleeva. Photopharmacology: A brief review using the control of potassium channels as an example. *Neurosci. Behav. Physiol.*, 49:184–191, 2019.

75. Piermichele Kobauri, Frank J Dekker, Wiktor Szymanski, and Ben L Feringa. Rational design in photopharmacology with molecular photoswitches. *Angew. Chem.*, page e202300681, 2023.

76. Johannes Broichhagen and Joshua Levitz. Advances in tethered photopharmacology for precise optical control of signaling proteins. *Curr. Opin. Pharmacol.*, 63:102196, 2022.

77. Mikhail N Ryazantsev, Daniil M Strashkov, Dmitrii M Nikolaev, Andrey A Shtyrov, and Maxim S Panov. Photopharmacological compounds based on azobenzenes and azoheteroarenes: Principles of molecular design, molecular modelling, and synthesis. *Russ. Chem. Rev.*, 90(7):868, 2021.

78. Hiroyuki Ohtani, Mitsuru Ishikawa, Hiroyasu Itoh, Yoshihiro Takiguchi, Tsuneyuki Urakami, and Yutaka Tsuchiya. Picosecond fluorescence spectroscopy of purple membrane in halobacterium halobium with a photon-counting streak camera. *Chem. Phys. Lett.*, 168(5):493–498, 1990.



https://doi.org/10.26434/chemrxiv-2023-3n1d0 **ORCID:** https://orcid.org/0000-0003-3413-1706 Content not peer-reviewed by ChemRxiv. **License:** CC BY-NC-ND 4.0

79. SL Shapiro, AJ Campillo, A Lewis, GJ Perreault, JP Spoonhower, RK Clayton, and W Stoeckenius. Picosecond and steady state, variable intensity and variable temperature emission spectroscopy of bacteriorhodopsin. *Biophys. J.*, 23(3):383–393, 1978.

80. Hiroyuki Ohtani, Takayoshi Kobayashi, Junichi Iwai, and Akira Ikegami. Picosecond and nanosecond spectroscopies of the photochemical cycles of acidified bacteriorhodopsin. *Biochemistry*, 25(11):3356–3363, 1986.

81. Takayoshi Kobayashi, Mamoru Terauchi, Tsutomu Kouyama, Masayuki Yoshizawa, and Makoto Taiji. Femtosecond spectroscopy of acidified and neutral bacteriorhodopsin. In *Laser Applications in Life Sciences*, volume 1403, pages 407–416. SPIE, 1991.

82. Tomas Gillbro and Arnd N Kriebel. Emission from secondary intermediates in the photocycle of bacteriorhodopsin at 77° k. *FEBS Lett.*, 79(1):29–32, 1977.

83. John TM Kennis, Delmar S Larsen, Kaoru Ohta, Marc T Facciotti, Robert M Glaeser, and Graham R Fleming. Ultrafast protein dynamics of bacteriorhodopsin probed by photon echo and transient absorption spectroscopy. *J. Phys. Chem. B*, 106(23):6067–6080, 2002.

84. Joel M Kralj, Adam D Douglass, Daniel R Hochbaum, Dougal Maclaurin, and Adam E Cohen. Optical recording of action potentials in mammalian neurons using a microbial rhodopsin. *Nat. Methods*, 9(1):90–95, 2012.

85. Alfons Penzkofer, Arita Silapetere, and Peter Hegemann. Absorption and emission spectroscopic investigation of the thermal dynamics of the archaerhodopsin 3 based fluorescent voltage sensor quasar1. *Int. J. Mol. Sci.*, 20(17):4086, 2019.

86. Daniel R Hochbaum, Yongxin Zhao, Samouil L Farhi, Nathan Klapoetke, Christopher A Werley, Vikrant Kapoor, Peng Zou, Joel M Kralj, Dougal Maclaurin, Niklas Smedemark-Margulies, et al. All-optical electrophysiology in mammalian neurons using engineered microbial rhodopsins. *Nat. Methods*, 11(8):825–833, 2014.

87. Alfons Penzkofer, Arita Silapetere, and Peter Hegemann. Absorption and emission spectroscopic investigation of the thermal dynamics of the archaerhodopsin 3 based fluorescent voltage sensor archon2. *Int. J. Mol. Sci.*, 21(18):6576, 2020.

88. R Scott McIsaac, Martin KM Engqvist, Timothy Wannier, Adam Z Rosenthal, Lukas Herwig, Nicholas C Flytzanis, Eleonora S Imasheva, Janos K Lanyi, Sergei P Balashov, Viviana Gradinaru, et al. Directed evolution of a far-red fluorescent rhodopsin. *Proc. Natl. Acad. Sci. U.S.A.*, 111(36):13034–13039, 2014.

89. Martin O Lenz, Robert Huber, Bernhard Schmidt, Peter Gilch, Rolf Kalmbach, Martin Engelhard, and Josef Wachtveitl. First steps of retinal photoisomerization in proteorhodopsin. *Biophys. J.*, 91(1):255–262, 2006.

90. Martin KM Engqvist, R Scott McIsaac, Peter Dollinger, Nicholas C Flytzanis, Michael Abrams, Stanford Schor, and Frances H Arnold. Directed evolution of gloeobacter violaceus rhodopsin spectral properties. *J. Mol. Biol.*, 427(1):205–220, 2015.

91. Srividya Ganapathy, Xin Meng, Delizzia Mossel, Mels Jagt, and Daan Brinks. Expanding the family of genetically encoded voltage indicators with a candidate heliorhodopsin exhibiting near-infrared fluorescence. *J. Biol. Chem.*, 299(6), 2023.



https://doi.org/10.26434/chemrxiv-2023-3n1d0 **ORCID:** https://orcid.org/0000-0003-3413-1706 Content not peer-reviewed by ChemRxiv. **License:** CC BY-NC-ND 4.0

92. Rinat Rozin, Amir Wand, Kwang-Hwan Jung, Sanford Ruhman, and Mordechai Sheves. ph dependence of anabaena sensory rhodopsin: retinal isomer composition, rate of dark adaptation, and photochemistry. *J. Phys. Chem. B*, 118(30):8995–9006, 2014.

93. Alexandre Cheminal, Jérémie Léonard, SY Kim, K-H Jung, H Kandori, and Stefan Haacke. Steady state emission of the fluorescent intermediate of anabaena sensory rhodopsin as a function of light adaptation conditions. *Chem. Phys. Lett.*, 587:75–80, 2013.

94. Alexandre Cheminal, Jérémie Léonard, So-Young Kim, Kwang-Hwan Jung, Hideki Kandori, and Stefan Haacke. 100 fs photo-isomerization with vibrational coherences but low quantum yield in anabaena sensory rhodopsin. *Phys. Chem. Chem. Phys.*, 17(38):25429–25439, 2015.

95. Hideki Kandori, Keitaro Yoshihara, Hiroaki Tomioka, and Hiroyuki Sasabe. Primary photochemical events in halorhodopsin studied by subpicosecond time-resolved spectroscopy. *J. Phys. Chem.*, 96(14):6066–6071, 1992.

96. Hans-Joachim Polland, MA Franz, Wolfgang Zinth, Wolfgang Kaiser, P Hegemann, and Dieter Oesterhelt. Picosecond events in the photochemical cycle of the light-driven chloride-pump halorhodopsin. *Biophys. J.*, 47(1):55–59, 1985.

97. T Arlt, S Schmidt, W Zinth, U Haupts, and D Oesterhelt. The initial reaction dynamics of the light-driven chloride pump halorhodopsin. *Chem. Phys. Lett.*, 241(5-6):559–565, 1995.

98. I Lutz, A Sieg, AA Wegener, M Engelhard, I Boche, M Otsuka, D Oesterhelt, J Wachtveitl, and W Zinth. Primary reactions of sensory rhodopsins. *Proc. Natl. Acad. Sci. U.S.A.*, 98(3):962–967, 2001.

99. Partha Malakar, Ishita Das, Sudeshna Bhattacharya, Andrew Harris, Mordechai Sheves, Leonid S Brown, and Sanford Ruhman. Bidirectional photochemistry of antarctic microbial rhodopsin: Emerging trend of ballistic photoisomerization from the 13-cis resting state. *J. Phys. Chem. Lett.*, 13(34):8134–8140, 2022.

100. Hideki Kandori, Yuji Furutani, Shoko Nishimura, Yoshinori Shichida, Haik Chosrowjan, Yutaka Shibata, and Noboru Mataga. Excited-state dynamics of rhodopsin probed by femtosecond fluorescence spectroscopy. *Chem. Phys. Lett.*, 334(4-6):271–276, 2001.

101. AG Doukas, MR Junnarkar, RR Alfano, RH Callender, and V Balogh-Nair. The primary event in vision investigated by time-resolved fluorescence spectroscopy. *Biophys. J.*, 47(6):795–798, 1985.

102. Anne P Rasmussen, Elisabeth Gruber, Ricky Teiwes, Mordechai Sheves, and Lars H Andersen. Spectroscopy and photoisomerization of protonated schiff-base retinal derivatives in vacuo. *Phys. Chem. Chem. Phys.*, 23(48):27227–27233, 2021.

103. Hideki Kandori and Hiroyuki Sasabe. Excited-state dynamics of a protonated schiff base of all-trans retinal in methanol probed by femtosecond fluorescence measurement. *Chem. Phys. Lett.*, 216(1-2):126–172, 1993.

104. SM Bachilo, SL Bondarev, and T Gillbro. Fluorescence properties of protonated and unprotonated schiff bases of retinal at room temperature. *J. Photochem. Photobiol. B, Biol.*, 34(1):39–46, 1996.



https://doi.org/10.26434/chemrxiv-2023-3n1d0 **ORCID:** https://orcid.org/0000-0003-3413-1706 Content not peer-reviewed by ChemRxiv. **License:** CC BY-NC-ND 4.0

105. Stephan L Logunov, Li Song, and Mostafa A El-Sayed. Excited-state dynamics of a protonated retinal schiff base in solution. *J. Phys. Chem.*, 100(47):18586–18591, 1996.

106. Hideki Kandori, Yuko Katsuta, Masayoshi Ito, and Hiroyuki Sasabe. Femtosecond fluorescence study of the rhodopsin chromophore in solution. *J. Am. Chem. Soc.*, 117(9):2669–2670, 1995.



https://doi.org/10.26434/chemrxiv-2023-3n1d0 **ORCID:** https://orcid.org/0000-0003-3413-1706 Content not peer-reviewed by ChemRxiv. **License:** CC BY-NC-ND 4.0